AAS 21-433

MODELING AND SIMULATION OF ROTARY SLOSHING IN LAUNCH VEHICLES

Jeb S. Orr*

The nonlinear dynamics of propellant sloshing during orbital ascent are usually neglected in the flight control analysis of large boost vehicles under the assumption that the viscous damping of the fluid is sufficient to suppress nonlinear phenomena and confine the fluid to small, planar free surface displacements. In this case, the sloshing dynamics can be modeled using a spring-mass-damper or linearized pendulum mechanical analog. However, large, smooth-wall tanks without significant internal hardware or ring baffles are still susceptible to nonlinear effects. In particular, rotary sloshing can present a risk to flight control as it involves the formation of a stable limit cycle which can lead to undesirable roll coupling. The underlying phenomena of jump resonance does not manifest in linear models, but can be reproduced using a nonlinear spherical pendulum or the Bauer paraboloid model developed during the Apollo/Saturn program. In this paper, a detailed analysis of the rotary sloshing dynamics of these mechanical analogs is presented, and discussed in the context of flight control stability. High-fidelity simulations of a representative boost vehicle are used to verify the semi-analytical predictions of the nonlinear dynamic response.

1 INTRODUCTION

Propellant motion, or "slosh," and its effects on the dynamics of an ascending rocket has proven to be one of the most formidable challenges in the design of flight control systems for liquid-propelled rockets. In the case of space launch vehicles, the motion of propellant sloshing within the fuel tanks is of great significance to the design as often more than 90% of the vehicle's liftoff mass is liquid propellant. The moving propellant appears to the rocket body and its control system as a lightly-damped moving mass, which, depending on the vehicle configuration, may be difficult to stabilize while maintaining sufficiently fast control response.

In the late 1950s and early 1960s, a significant research effort was dedicated to understanding the dynamics of sloshing propellants as the size of liquid-propellant boosters began to grow to massive scales. Techniques that would now be considered mass-inefficient and unconventional, such as radially segmented tanks, floating metallic damper cans, and accordion baffles - used in the oxidizer tanks of NASA's Saturn I and IB launch vehicles - have now been replaced by simple ring baffles. Ring baffles, combined with linear and nonlinear analysis of the vehicle dynamics, often reduce risk of propellant instability to an acceptable level.

Propellant slosh is, however, not a solved problem. Sloshing propellant is usually modeled as a linearized pendulum or an equivalent spring, mass, and damper coupled to the vehicle rigid and elastic degrees of freedom such that the force and moment response of the mechanical analog matches that of test-correlated semi-empirical models of a rigid tank. The portion of the equivalent liquid

*Principal Staff, Flight Systems (Mclaurin Aerospace - AMA TEAMS 3), Knoxville, TN, jeb.orr@mclaurin.aero

mass that is not in motion is lumped into the rigid-body mass. The properties of the mechanical analog change as a function of propellant remaining and the vehicle acceleration. Such a strictly linear model has two fundamental limitations: it is not valid near the natural frequencies of the propellant modes (at resonance), and it does not capture the important coupling between the degrees of freedom of the lateral modes. The latter, which is the topic of this paper, can lead to stable rotary limit cycles in the fluid response. This phenomenon is known as *rotary slosh*.

Analytical and experimental investigations by Miles[1] and Hutton[2] concluded that the qualitative response of the spherical pendulum to periodic forcing is very similar to that of a cylindrical tank of fluid. The spherical pendulum became a natural target of investigation in the search for a mechanical analog. Hutton's experimental data, published in 1963 and supported by Miles's analytical work on the nonlinear pendulum dynamics, showed that a fluid in a cylindrical container under constant sinusoidal excitation contains essentially four fundamental response regions, depending on input frequency: (1) stable, in-plane motion or unstable high-amplitude motion below the resonant frequency, (2) chaotic motion near resonance, (3) rotary motion in a narrow band just above resonance, and (4) either stable rotary or planar motion above resonance. At higher excitation amplitudes or for initial conditions corresponding to large angular displacements, the pendulum exhibits the same nonlinear phenomena of stiffening, softening, and jump resonance. However, when compared with the fluid test data, the out-of-plane (rotary) dynamics of the pendulum did not exhibit the proper amplitude ratio at frequencies above resonance. This limitation was highlighted by Bauer et al.[3] in 1965, who then proposed a modified mechanical model derived from the same linear potential theory used to develop the spring-mass-damper models of the fluid. Importantly, Bauer introduced a variable nonlinear spring which can be adjusted to match the test data. Expanded to third order, this model still has the form of the *Duffing equation,* which also arises in the analysis of the spherical pendulum. This structure allows the use of harmonic balance techniques to produce semi-analytical solutions.

2 TRADITIONAL MECHANICAL MODELS

A spring-mass or pendulum mechanical analog is the established method for modeling liquid dynamics in boost vehicles, primarily for axisymmetric, cylindrical tanks in conditions where surface tension effects can be ignored ($Bo > 100$). Spring-mass parameters can be derived for many geometries, including rectangular, conical, and radially or annular segmented tanks. Usually an analyst is concerned only with the first one to three antisymmetric free surface modes, although the first mode is always a driving factor for flight dynamics. Under the assumptions of an irrotational, inviscid incompressible fluid in a rigid, flat-bottomed cylindrical tank, the fluid antisymmetric mode frequencies are given by[4]

$$\omega_n^2 = \frac{\bar{g}}{a}\epsilon_n \tanh\left(\epsilon_n \frac{h}{a}\right) \tag{1}$$

where $\epsilon_n \triangleq \{\epsilon \ni J_1'(\epsilon) = 0\}$ are the roots of the first derivative of J_1, a Bessel function of the first kind;

$$\epsilon_n = 1.841,\ 5.332,\ 8.536,\ 11.706,\ \ldots, \tag{2}$$

the liquid height is h, and the tank radius is a. The value $\bar{g}$ is the absolute axial acceleration in units consistent with h and a. For tanks without flat bottoms, this relationship is accurate for any section of the tank where $h \gtrsim 2a$, since the value of $\tanh\left(\epsilon_n \frac{h}{a}\right) \to 1$.

The resultant spring-mass parameters can be extracted via equivalence analysis of the forced response; the sloshing mass is

$$m_n = 2m_L \frac{\tanh\left(\epsilon_n \frac{h}{a}\right)}{\epsilon_n \frac{h}{a}\left(\epsilon_n^2 - 1\right)} \tag{3}$$

where m_L is the total liquid mass; by mechanical analogy, the spring and damper values $k_n = m_n\omega_n^2$ and $d_n = 2m_n\zeta_n\omega_n$, respectively. The location of the sloshing mass with respect to the liquid free surface is resolved to provide an equivalent force and moment on the rigid tank;

$$l_n = \frac{a}{\epsilon_n} \tanh\left(\epsilon_n \frac{h}{a}\right). \tag{4}$$

The pendulum length is given by

$$L_n = \frac{a}{\epsilon_n} \coth\left(\epsilon_n \frac{h}{a}\right) \tag{5}$$

and the pivot location with respect to the tank bottom is

$$l_{pn} = h - l_n + L_n. \tag{6}$$

It should be noted that these parameters are valid only within the range of liquid heights that are within the barrel section of the tank. Additional corrections must be applied when the free surface reaches the upper and lower domes.

Of course, the spring-mass and linearized pendulum models are equivalent, if the pendulum is expanded in a first-order Taylor series about small angles. Both models will produce the same force and moment response on the tank, subject to the necessary transformation of the parameters to account for the change in hinge point. For the linearized spring-mass model, the relative acceleration $\ddot{\boldsymbol{\delta}}_s$ of the first liquid mode slosh mass m_1 is incorporated into the nonlinear angular motion equations, for example, as

$$\mathbf{I}_T\dot{\boldsymbol{\omega}} + m_1\mathbf{r}_s^{\times}\ddot{\boldsymbol{\delta}}_s = -\boldsymbol{\omega}^{\times}\mathbf{I}_T\boldsymbol{\omega} - 2m_1\left(\mathbf{r}_s + \boldsymbol{\delta}_s\right)^{\times}\boldsymbol{\omega}^{\times}\dot{\boldsymbol{\delta}}_s - m_1\boldsymbol{\delta}_s^{\times}\bar{\mathbf{g}} \tag{7}$$

where $\mathbf{I}_T$ is the total vehicle inertia, $\boldsymbol{\omega}$ is the body angular rate, and $\bar{\mathbf{g}}$ is the quasi-steady axial acceleration. The RHS of Equation 7 contains the usual gyroscopic and Coriolis terms, along with a slosh *offset effect* that arises when using a simplified, quasi-steady mass matrix.[5] This simplified expression is adequate for a *linear* slosh model and *nonlinear* vehicle dynamics, under the assumption that the sloshing displacements are small and the vehicle is not spinning. This is, however, not a *nonlinear slosh model*. While it is possible to incorporate a complete dynamic and kinematic description of a nonlinear spherical pendulum into the vehicle dynamics, doing so often introduces significant simulation complexity and it is sufficient to model a "loosely coupled" local spherical pendulum. In the discussion that follows, it will be assumed that only the lowest-frequency antisymmetric liquid mode (m_1) is modeled, and $m_s = m_1$, $k_s = k_1$, etc.

2.1 Analysis of the Pendulum Model

The planar pendulum can be analyzed using a Taylor expansion of the pendulum dynamics given by

$$\ddot{\alpha} + 2\zeta p\dot{\alpha} + p^2 \sin\alpha = u\cos\alpha \tag{8}$$

where $u = \epsilon\Omega^2\cos\Omega t$ is a small periodic input, ζ is a viscous damping factor, α is the pendulum angle, and $p = \sqrt{\bar{g}/L_s}$ is the frequency parameter. Note that in contrast with the above discussion,

ϵ is used to represent a small quantity. The pendulum frequency p is not necessarily equal to the input frequency Ω. Taylor expansion of Equation 8 yields the Duffing equation;

$$\ddot{\alpha} + 2\zeta p\dot{\alpha} + p^2\alpha - \frac{1}{6}p^2\alpha^3 = \epsilon\Omega^2\cos\Omega t. \tag{9}$$

The fourth term on the LHS is a nonlinear, third-order spring, and the remaining system is a linear constant-coefficient ordinary differential equation with a resonant frequency equal to $p\sqrt{1-2\zeta^2} \approx p$. It was shown by Miles[1] that near resonance, an approximate solution is given by

$$\alpha(t) \approx \epsilon^{\frac{1}{3}} a\cos\Omega t + \epsilon a_3\cos 3\Omega t + O(\epsilon^{\frac{5}{3}}) \tag{10}$$

where a and a_3 are constants to be determined. Like the free pendulum, the solutions consist of odd harmonics. Introducing frequency and amplitude normalization, the frequency response of the pendulum first harmonic in the vicinity of resonance can be described in terms of its amplitude ratio A/ϵ and its frequency ratio η, where $A = a\epsilon^{1/3}$ and $\eta = \Omega/p$, respectively. Such an analysis provides a measure of the nonlinear frequency response of the system to periodic inputs. A similar approach is used to derive the response curves for the out-of-plane dynamics, and the response with nonzero damping ζ.

For a linear system with natural frequency p subject to the same inputs, it can be shown that in terms of the frequency ratio η, the magnitude response of the linear system is given by

$$|H(j\eta)| = \left(1 + 4\eta^2\zeta^2 - 2\eta^2 + \eta^4\right)^{-\frac{1}{2}} \tag{11}$$

and therefore the linear resonance curve can be compared with the nonlinear first harmonic resonance curve using

$$a_L = \epsilon\,|H(j\eta)|\,\epsilon^{-\frac{1}{3}} = |H(j\eta)|\,\epsilon^{\frac{2}{3}}. \tag{12}$$

2.2 Bauer Nonlinear Model

Bauer et al.[3] derived an improved nonlinear model, based directly on the solution of the Laplace PDE governing the fluid dynamics in the container. By integrating over the fluid displacement, Bauer noted that the axial center of mass displacement of the first mode is given by

$$x_s = -\frac{C_s}{2a}r_s^2 = -\frac{C_s}{2a}\left(y_s^2 + z_s^2\right)$$

where the slosh parameter is $C_s = \epsilon_1\tanh\left(\epsilon_1\frac{h}{r}\right)$. The axial displacement of the slosh mass acts as if it is constrained to a parabolic surface. Bauer then conjectured a 2-degree-of-freedom model, shown here without viscous damping, having the form

$$\ddot{y}_s + \frac{C_s^2}{a^2}\left(y_s^2\ddot{y}_s + y_s\dot{y}_s^2 + y_sz_s\ddot{z}_s + y_s\dot{z}_s^2\right) + \omega_s^2\left[1 + \frac{\alpha_s}{a^2}\left(y_s^2 + z_s^2\right)\right]y_s = u_y \tag{13}$$

$$\ddot{z}_s + \frac{C_s^2}{a^2}\left(z_s^2\ddot{z}_s + z_s\dot{z}_s^2 + z_sy_s\ddot{y}_s + z_s\dot{y}_s^2\right) + \omega_s^2\left[1 + \frac{\alpha_s}{a^2}\left(y_s^2 + z_s^2\right)\right]z_s = u_z. \tag{14}$$

The second term in Equations 13 and 14 is the paraboloid constraint of the slosh mass, and the third term contains a nonlinear spring with an adjustable parameter α_s. A schematic of such a model is shown in Figure 1. By inspection, this model collapses to a linear spring-mass system if truncated to first order in the displacement and velocity. This is convenient for implementation in linear stability models. Importantly, the coupling of the y and z degrees of freedom is implicit in the constraint, and does not require external kinematic equations.

The harmonic response of the spherical pendulum is shown in Figure 2 along with the Bauer model response ($\alpha_s = \frac{2}{3}$) and a portion of Hutton's test data for a water tank having a radius of about 6 inches. In Bauer's model, the equivalent wave amplitude at the wall is computed from the radial displacement of the sloshing mass using

$$\bar{x}_W = \frac{2rC_s}{\epsilon_1^2 - 1} r_s. \tag{15}$$

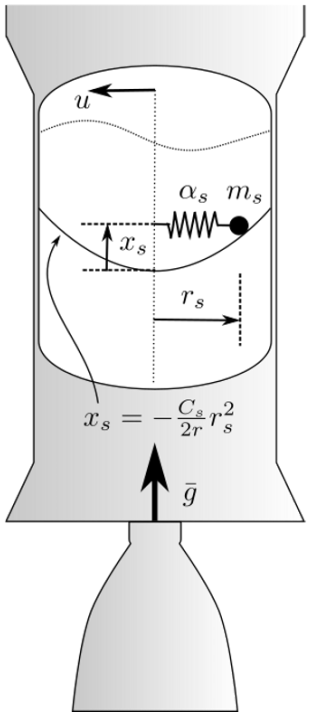

Figure 1. Bauer mechanical model

2.3 Harmonic Analysis

As was shown by Miles, the planar response is partitioned into four primary branches (I-IV). Branch I is the low-amplitude stable response below resonance. The linear model and the nonlinear model agree well for $\eta < 0.95$ and $\eta > 1.05$ (see Figure 3). Near resonance, the nonlinear system exhibits the characteristic folding behavior, where the amplitude response is multi-valued at a given input frequency. Branches II and III are unstable; that is, it is not possible to develop a limit cycle on an unstable branch, and the response will collapse onto a stable branch.

Branch VI is the stable rotary branch. Along branch VI, the response is stable, periodic, high-amplitude, and contains two components along the two response degrees of freedom that are 90 degrees out of phase. In the region just above resonance, there is only a rotary solution.

One characteristic that arises applying the Ritz averaging method to the Bauer model is that the nonplanar branch exhibits two characteristic curves which converge to a single amplitude at higher frequency. These curves represent the different in-plane and out-of-plane amplitudes, representing a slightly elliptical response of the system at low amplitudes when close to the linear resonant frequency. This asymmetry is difficult to discern in the test data but is readily reproduced in nonlinear simulation using carefully controlled initial conditions.

Bauer hinted in his original report[3] that the introduction of damping does not significantly change the characteristics of the rotary branch (VI). The author conjectures that Bauer and his colleagues did not assert this conclusively since the solution for the damped branch VI requires an iterative numerical method, which is now feasible (albeit still difficult) using modern computational techniques.

A comparison of the effect of 1% viscous damping on the linear and nonlinear resonances is shown in Figure 3. Damping has the important property that for the in-plane response, the amplitude is decreased to a point that the linear and nonlinear models are not substantially different. However, the out-of-plane response is essentially unaffected by damping, and it has been observed that the rotary limit cycle may indeed be more stable (in an average potential energy sense) than the planar limit cycle at the same driving frequency.[3] This is an important result; the Bauer model incorporates a global viscous dissipation term that is proportional to the velocity of the slosh mass with respect to the paraboloid.

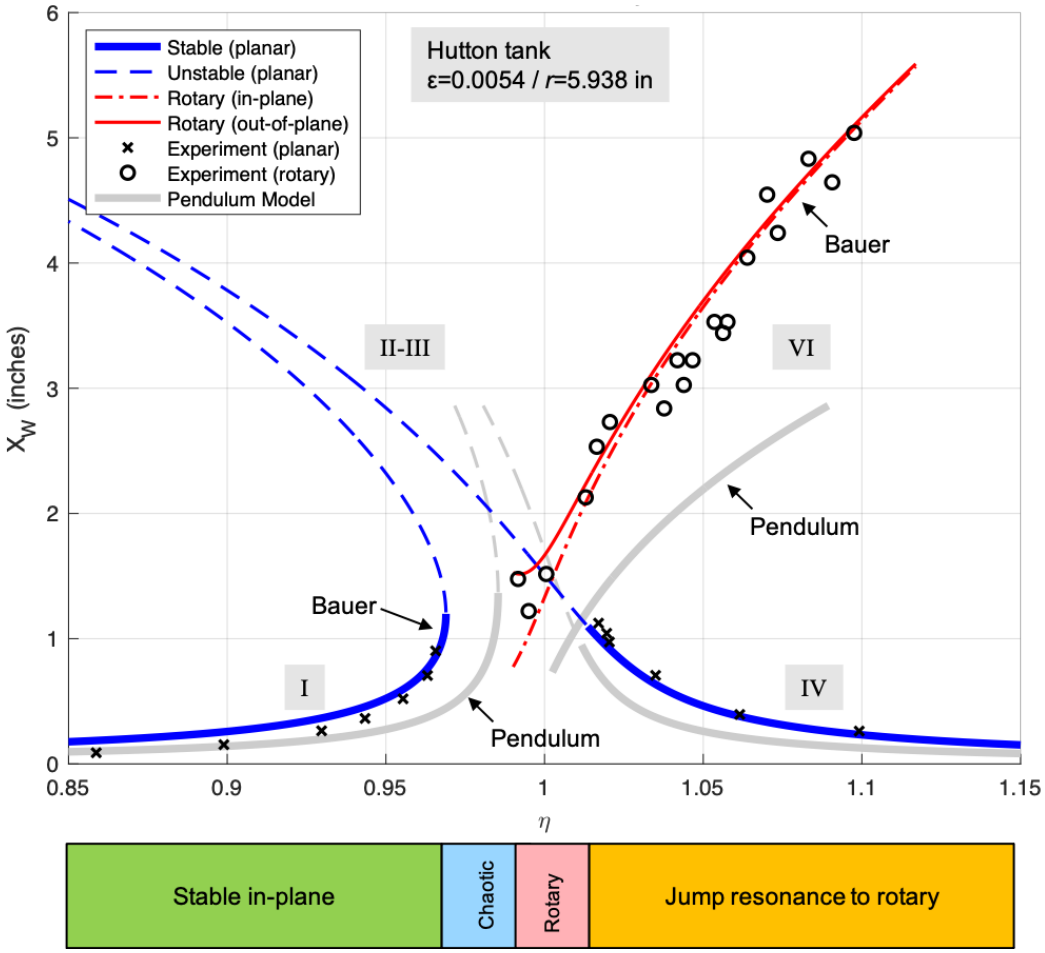

Figure 2. Spherical pendulum and Bauer resonance curves

3 ADVANCED ROTARY MODEL

Bauer's mechanical model (Equations 13 and 14) can be modified and extended for incorporation into modern flight dynamics simulations. While mechanical model parameters can be based on linear potential theory using Bessel functions for analytic boundary conditions, Lomen[6] introduced a numerical method to determine the parameters that is now common in practice. This method is more general in the sense that it can determine the natural frequencies for an arbitrary container that is a body of revolution, and these natural frequencies and slosh masses are used directly in the model. The liquid modal parameter $C_s = \epsilon_1 \tanh\left(\epsilon_1 \frac{h}{a}\right)$ is related to the natural frequency;

$$\omega_s^2 = \frac{g}{a}\epsilon_1 \tanh\left(\epsilon_1 \frac{h}{a}\right) = \frac{\bar{g}}{a} \tag{16}$$

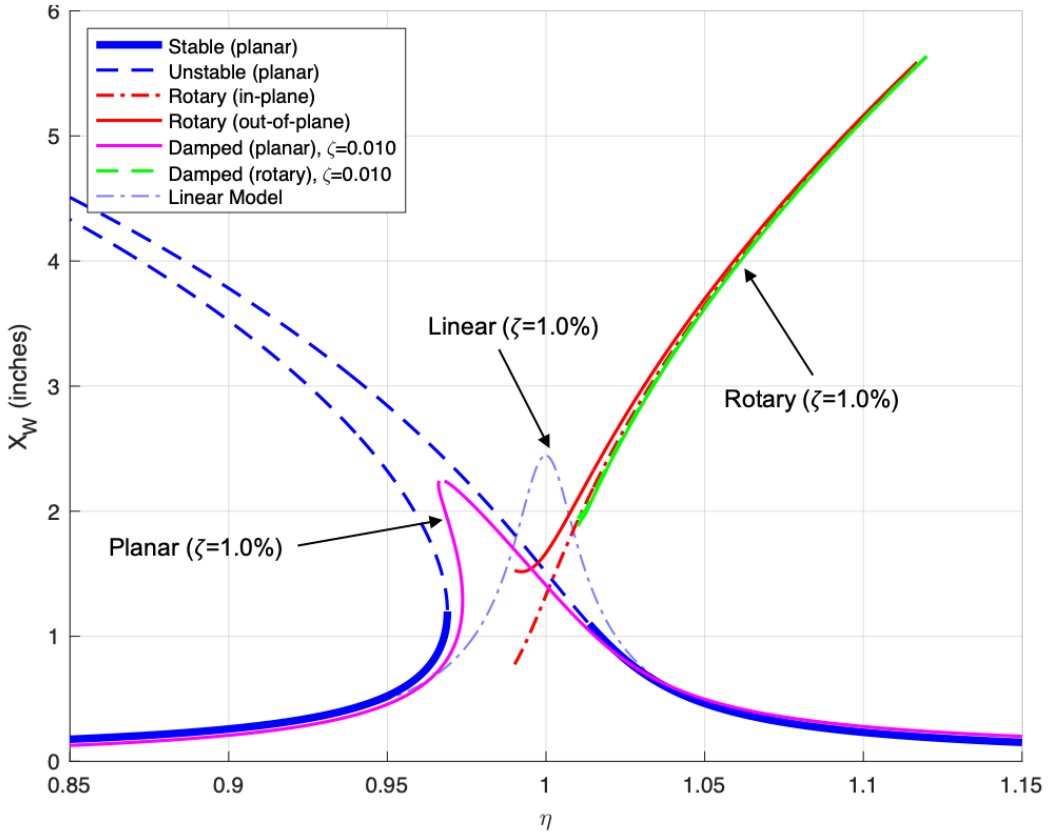

Figure 3. Damped and undamped resonance curves

thus $\frac{C_s^2}{a^2} = \frac{\omega_s^4}{\bar{g}^2}$ where ω_s is the g-scaled natural frequency, and the spring coefficient is given by $\alpha_s = \frac{k_s a^2}{m_s \omega_s^2}$. Using these relationships, Bauer's equations (with damping) are

$$\ddot{z}_s + \frac{\omega_s^4}{\bar{g}^2}\left(z_s^2\ddot{z}_s + z_s y_s \ddot{y}_s\right) = -\frac{\omega_s^4}{\bar{g}^2}\left(z_s\dot{z}_s^2 + z_s\dot{y}_s^2\right) - 2\omega_s\zeta_s\left[\dot{z}_s + \frac{\omega_s^4}{\bar{g}^2}\left(z_s^2\dot{z}_s + z_s y_s \dot{y}_s\right)\right] - \omega_s^2\left[1 + \frac{\alpha_s}{a^2}r_s^2\right]z_s + u_z \quad (17)$$

$$\ddot{y}_s + \frac{\omega_s^4}{\bar{g}^2}\left(y_s^2\ddot{y}_s + y_s z_s \ddot{z}_s\right) = -\frac{\omega_s^4}{\bar{g}^2}\left(y_s\dot{y}_s^2 + y_s\dot{z}_s^2\right) - 2\omega_s\zeta_s\left[\dot{y}_s + \frac{\omega_s^4}{\bar{g}^2}\left(y_s^2\dot{y}_s + y_s z_s \dot{z}_s\right)\right] - \omega_s^2\left[1 + \frac{\alpha_s}{a^2}r_s^2\right]y_s + u_y. \quad (18)$$

It is possible to write these coupled equations in matrix form as $\mathcal{M}\ddot{\boldsymbol{\delta}}_s = \mathbf{q}$ with $\boldsymbol{\delta}_s = \begin{bmatrix} y_s & z_s \end{bmatrix}^T$ and $r_s = \|\boldsymbol{\delta}_s\|$ with

$$\mathcal{M} = \begin{bmatrix} 1 + \frac{\omega_s^4}{\bar{g}^2}y_s^2 & \frac{\omega_s^4}{\bar{g}^2}y_s z_s \\ \frac{\omega_s^4}{\bar{g}^2}y_s z_s & 1 + \frac{\omega_s^4}{\bar{g}^2}z_s^2 \end{bmatrix} = \mathbf{I} + \frac{\omega_s^4}{\bar{g}^2}\boldsymbol{\delta}_s\boldsymbol{\delta}_s^T. \quad (19)$$

The simplified vector form can be written as

$$\left[\mathbf{I} + \frac{\omega_s^4}{\bar{g}^2}\boldsymbol{\delta}_s\boldsymbol{\delta}_s^T\right]\ddot{\boldsymbol{\delta}}_s = \ -2\omega_s\zeta_s\dot{\boldsymbol{\delta}}_s \ - \omega_s^2\boldsymbol{\delta}_s - \frac{\omega_s^4}{\bar{g}^2}\left(\dot{r}_s^2 + 2\omega_s\zeta_s\boldsymbol{\delta}_s^T\dot{\boldsymbol{\delta}}_s\right)\boldsymbol{\delta}_s \ -\omega_s^2\tfrac{\alpha_s}{a^2}r_s^2\boldsymbol{\delta}_s \ + \mathbf{u}. \quad (20)$$

The input term $\mathbf{u}$ contains the forcing terms arising from coupling with the nonlinear vehicle dynamic equations; that is,

$$\mathbf{u} = \left\{-\mathbf{a}_b + \mathbf{r}_s^\times\dot{\boldsymbol{\omega}} + \boldsymbol{\omega}^\times\mathbf{r}_{sj}^\times\boldsymbol{\omega} - 2\boldsymbol{\omega}^\times\dot{\boldsymbol{\delta}}_{sj}\right\}_{2,3} \quad (21)$$

where $\mathbf{a}_b$, $\dot{\boldsymbol{\omega}}$ are the body frame translational and angular acceleration, respectively, and the remaining terms are centripetal and Coriolis effects of the moving body frame. Elasticity is not included in Equation 21 but these effects are incorporated in high-fidelity models.[5] For simulation, the Bauer model can be treated as a traditional spring-mass-damper model with additional nonlinear terms; the only required additional data are the spring parameter (typically $\alpha_s = \frac{2}{3}$) and the tank radius a. Numerical analysis of this model's response as a standalone module agrees nearly exactly with the predictions of Figure 2, notably reproducing, with remarkable accuracy, the elliptical rotation predicted by the Ritz method. This confirms the validity of the series approximations used in deriving the approximate solutions.

An improvement to the Bauer model is straightforward, noting that in practice, damping mechanisms such as ring baffles do not provide global damping but instead are dependent on the direction of the slosh wave with respect to the wall. That is, in a smooth-walled tank, an ideal ring baffle provides damping approximately along the radial velocity direction but very little dissipation for motion tangent to the wall. Thus, an established rotary slosh wave with an approximately constant wave amplitude will not dissipate energy at the same rate as one having a strong periodic radial component. This can be approximated in the mechanical model by incorporating *split damping*, where a smooth-wall viscous damping value is applied to the tangential component of the sloshing velocity but a baffle damping value is applied to the radial component.

The implementation of split damping can be accomplished with a temporary transformation to polar coordinates. The dissipation force in Equation 20 can be written as $\mathbf{Q}_d = -2\omega_s\zeta_s\dot{\boldsymbol{\delta}}_p$ with

$$\dot{\boldsymbol{\delta}}_p = \left[\mathbf{I} + \frac{\omega_s^4}{\bar{g}^2}\boldsymbol{\delta}_s\boldsymbol{\delta}_s^T\right]\dot{\boldsymbol{\delta}}_s \quad (22)$$

where $\dot{\boldsymbol{\delta}}_p$ is the paraboloid-relative velocity and $\dot{\boldsymbol{\delta}}_s$ is the slosh mass velocity. The paraboloid-relative velocity is used, consistent with Bauer's assumptions, in that the velocity normal to the wall increases as a function of wave amplitude. This is consistent with contemporary models of nonlinear dissipation in lateral sloshing.[7]

By determining the radial and tangential velocities in mixed coordinates,

$$\dot{r}_p = \dot{y}_p\cos\theta_p + \dot{z}_p\sin\theta_p \quad (23)$$

$$\dot{\theta}_p = \frac{1}{r_p}\left(\dot{z}_p\cos\theta_p - \dot{y}_p\sin\theta_p\right). \quad (24)$$

It can be shown that by applying a radial damping ζ_r to $\dot{r}_p$ and a tangential damping ζ_t to $\dot{\theta}_p$, the dissipation force can be written as

$$\mathbf{Q}_d = -2\omega_s\mathbf{R}_d\left[\mathbf{I} + \frac{\omega_s^4}{\bar{g}^2}\boldsymbol{\delta}_s\boldsymbol{\delta}_s^T\right]\dot{\boldsymbol{\delta}}_s \quad (25)$$

with

$$\mathbf{R}_d = \frac{1}{r_s^2}\begin{bmatrix} \left(y_s^2\zeta_r + z_s^2\zeta_t\right) & y_s z_s\left(\zeta_r - \zeta_t\right) \\ y_s z_s\left(\zeta_r - \zeta_t\right) & \left(y_s^2\zeta_t + z_s^2\zeta_r\right) \end{bmatrix}. \tag{26}$$

Note that for $\zeta_r = \zeta_t$ the expression collapses to the usual Bauer damping model. The improved model with split damping is given by

$$\left[\mathbf{I} + \frac{\omega_s^4}{\bar{g}^2}\boldsymbol{\delta}_s\boldsymbol{\delta}_s^T\right]\ddot{\boldsymbol{\delta}}_s = -\omega_s^2\boldsymbol{\delta}_s - \left(\frac{\omega_s^4}{\bar{g}^2}\dot{r}_s^2 + \omega_s^2\frac{\alpha_s}{a^2}r_s^2\right)\boldsymbol{\delta}_s - 2\omega_s\mathbf{R}_d\left[\mathbf{I} + \frac{\omega_s^4}{\bar{g}^2}\boldsymbol{\delta}_s\boldsymbol{\delta}_s^T\right]\dot{\boldsymbol{\delta}}_s + \mathbf{u}. \tag{27}$$

4 SIMULATION ANALYSIS

The improved Bauer model was implemented and evaluated as a standalone tank model to assess the numerical response as compared with theory and test data from the Hutton series. In previously published data, only the test and analytical solutions were compared with an assumption of zero viscous damping. However, owing to the relatively small radius of Hutton's tank, the viscous damping is not insignificant. The smooth-wall log decrement damping for a cylindrical tank is given by

$$\delta \approx 5.23\nu^{1/2}a^{-3/4}\bar{g}^{-1/4} \tag{28}$$

where ν is the kinematic viscosity; the damping ratio is

$$\zeta = \left[1 + \left(\frac{2\pi}{\delta}\right)^2\right]^{-1/2} \tag{29}$$

yielding $\zeta = 0.184\%$ for the Hutton tank. Fortunately, the test conditions for Hutton's tank match data later published by Silverman and Abramson[8] validating Equation 28 for a 5.98 inch tank containing water.

Time domain simulation results are shown in Figures 4-6. In each of these cases, the initial fluid displacement is very nearly zero and the input is a constant sinusoidal acceleration consistent with the original test conditions ($\epsilon = 0.0054$). The radial wave amplitude is depicted with respect to time, along with a projection of the slosh mass within the tank; the constant radial wave amplitude from the test is shown in grey with the red portion used for Fourier analysis to extract the amplitude and phase response. The simulated regime is $\eta = 1.01$, in which the limit cycles involve pure rotary motion. A constant wave amplitude time history is indicative of a stable rotary limit cycle.

In Figure 4, the symmetric damping model is used with $\zeta = 0.184\%$, which readily converges to the condition predicted by the theory and confirmed by test. The limit cycle trajectory is clearly attractive with asymptotic convergence; the author conjectures that *radial* energy dissipation is actually required to stabilize the rotary limit cycle. In fact, in Figure 5, the radial damping is decreased to $\zeta_r = 0.02\%$, consistent with smooth-wall damping for a larger tank. It is apparent that while the initial transient has a shape similar to that shown in Figure 4, the limit cycle is not stable and is instead chaotic. This nonlinear behavior is counterintuitive to launch vehicle controls engineers versed in linear systems theory: in this case, the lack of dissipation precludes the formation of a dangerous limit cycle. Comparatively, in Figure 6, the radial damping is increased to $\zeta_r = 3.7\%$, in family with the damping produced near ring baffles. The response reaches the stable rotary limit cycle more quickly, confirming that rotary responses can occur even in well-damped tanks, given the correct combination of forcing function and initial conditions. In fact, related numerical experiments show that a transition from planar to stable rotary motion is possible even at damping ratios above $\zeta_r = 9\%$ at slightly higher drive amplitudes.

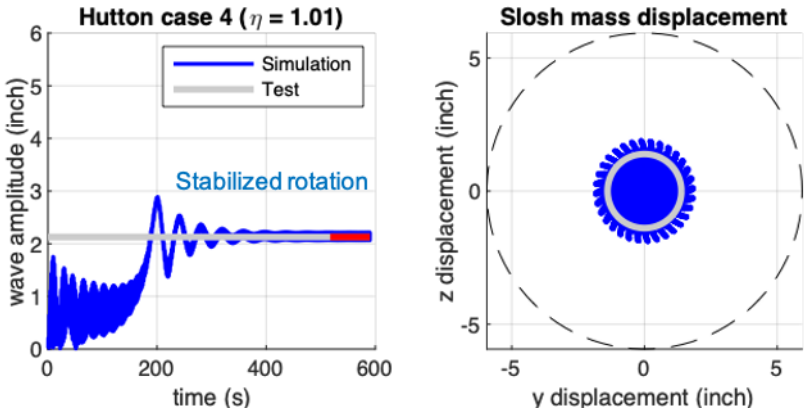

Figure 4. Hutton case 4, $\zeta_r = \zeta_t = 0.184\%$**.**

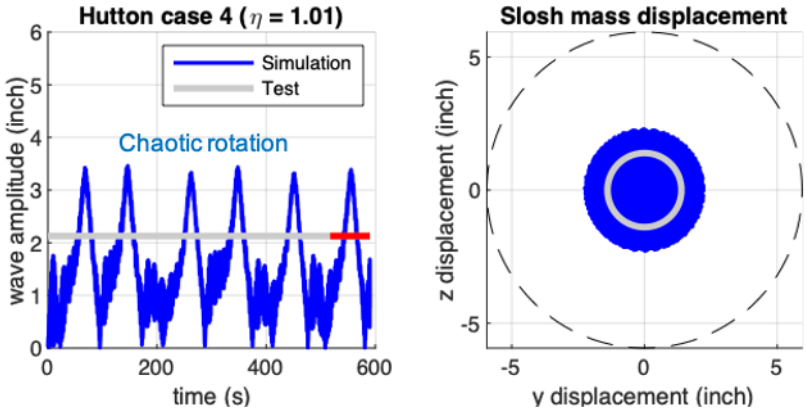

Figure 5. Hutton case 4, $\zeta_r = 0.184\%$**,** $\zeta_t = 0.02\%$**.**

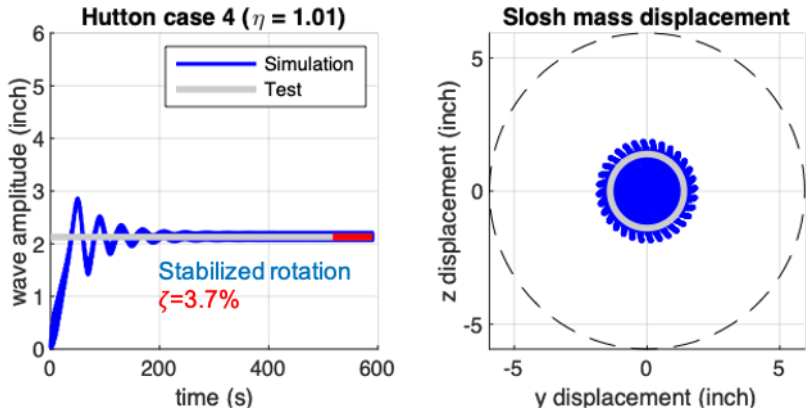

Figure 6. Hutton case 4, $\zeta_r = 3.7\%$**,** $\zeta_t = 0.184\%$**.**

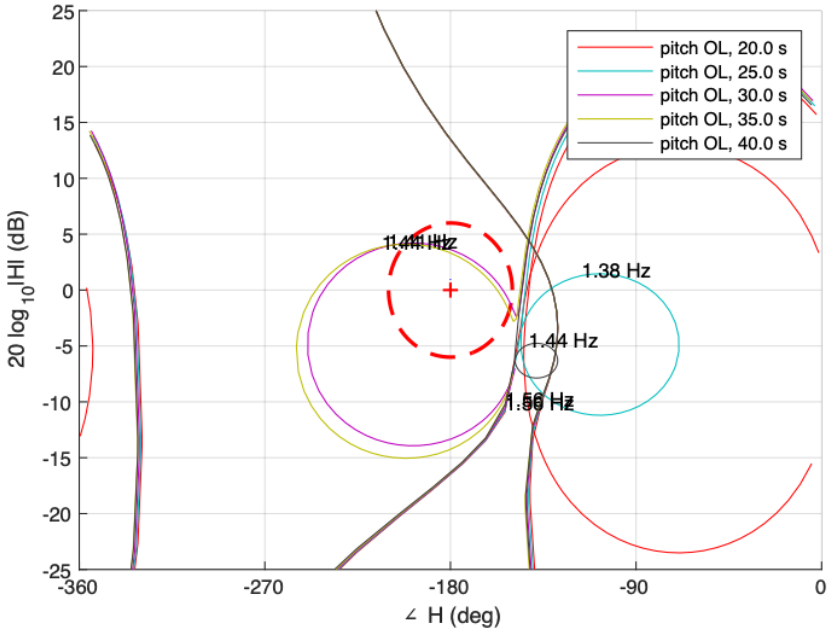

Figure 7. Slosh parameter dispersions yield unstable slosh-control coupling near T=30s.

A Monte Carlo analysis using the high-fidelity launch vehicle simulation DELTA (Dynamic Environment for Launch Trajectory Analysis) was used to assess the likelihood of rotary limit cycle development in a typical liquid-propellant rocket configuration when compared with a traditional pendulum model. Although statistically unlikely to occur, it was shown that in certain cases a slightly unstable,* lightly damped slosh mode having about $\zeta_r = 1\%$ radial damping could enter a stable rotary limit cycle that was not predicted using the pendulum model (Figures 7 and 8). The mechanism leading to rotary motion involves residual energy in the oxidizer tank from a guidance maneuver occurring some 20 seconds prior to the onset of the sloshing instability.

5 CONCLUSIONS

Propellant slosh continues to present a concern for launch vehicle dynamics and control, particularly as the launch vehicle industry pushes for increased performance, reduced integration overhead, and mass savings that can be realized by reducing the number of baffles and eliminating internal tank hardware. Certain tank geometries, particularly thin-wall pressure-stabilized tanks, may be more susceptible to the development of slosh instabilities in the unbaffled configuration. These tank designs lack the beneficial, approximately isotropic damping of an orthogrid/isogrid wall structure. Seemingly beneficial reductions in flight control design conservatism that allow for marginally stable or unstable sloshing dynamics should not be accepted without a thorough analysis in time domain simulation. As is suggested by the present analysis, the right combination of conditions, particularly large maneuvers, can produce a rotary limit cycle even in the presence of ring baffles. The use of advanced, test-correlated nonlinear models, such as the improved Bauer model, should be considered in the flight certification process when warranted to reduce risk.

*In the sense of linear autopilot analysis using a spring-mass damper.

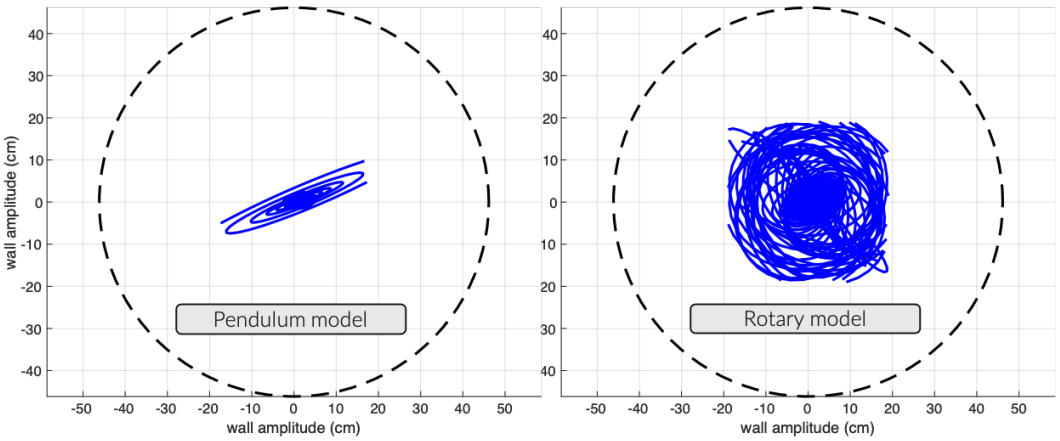

Figure 8. Monte Carlo 6-DoF simulation case identifies rotary motion not predicted by pendulum model.

ACKNOWLEDGEMENTS

This work was supported by the NASA Engineering and Safety Center (NESC) under contract 80LARC17C0003. The support of Neil Dennehy, Aron Wolf, Tannen VanZwieten, and the NESC GN&C Technical Discipline Team (TDT) is gratefully acknowledged. In addition, the author would like to thank Jing Pei of NASA LaRC for his insights in developing and improving the Bauer non-linear model.

REFERENCES

[1] Miles, J.W., Stability of Forced Oscillations of a Spherical Pendulum, Quarterly of Applied Mathematics Vol. 20, No. 1 (April 1962), pp. 21-32.

[2] Hutton, R., "An investigation of resonant, nonlinear, nonplanar free surface oscillations of a fluid," NASA TN-D-1870, 1963.

[3] Bauer, H.F., Clark, C.D., and Woodward, J.H., "Analytical Mechanical Model for the Description of the Rotary Propellant Sloshing Motion," Project A-767 Final Report, May 31, 1965.

[4] Fontenot, L. L., NASA CR-941, Dynamic Stability of Space Vehicles, Volume VII – The Dynamics of Liquids in Fixed and Moving Containers, March 1968.

[5] Barrows, T.M. and Orr, J.S., Dynamics_and_Simulation_of_Flexible_Rockets, Chapter 5, Elsevier/Academic Press, 2021.

[6] Lomen, D.O., "Liquid Propellant Sloshing in Mobile Tanks of Arbitrary Shape," NASA CR-222, 1965.

[7] VanZwieten, T.S. et al., "Nonlinear Slosh Damping Testing and Analysis for Launch Vehicle Propellant Tanks," AIAA SciTech 2020 Forum, Orlando, FL, AIAA 2020-2050, 6-10 January, 2020.

[8] Silverman, S., and Abramson, H.N., "Damping of Liquid Motions and Lateral Sloshing," NASA SP-106, Ch. 3, 1966.